

# Revelation of Fe(V)/Fe(IV) Involvement in the Fe(VI)–ABTS System: Kinetic Modeling and Product Analysis

Cong Luo, Manasa Sadhasivan, Juhee Kim, Virender K. Sharma,\* and Ching-Hua Huang\*



Cite This: *Environ. Sci. Technol.* 2021, 55, 3976–3987



Read Online

ACCESS |



Metrics & More



Article Recommendations



Supporting Information

**ABSTRACT:** To quantitatively probe iron intermediate species [Fe(V)/Fe(IV)] in Fe(VI) oxidation, this study systematically investigated the reaction kinetics of Fe(VI) oxidation of 2,2'-azino-bis(3-ethylbenzothiazoline-6-sulfonic)acid (ABTS) at different ratios of  $[ABTS]_0/[Fe(VI)]_0$  (i.e.,  $>1.0$ ,  $=1.0$ , and  $<1.0$ ) in pH 7.0 phosphate (10 mM)-buffered solution. Compared to the literature, a more comprehensive and robust kinetic model for the Fe(VI)–ABTS system including interactions between high-valent iron species [Fe(VI), Fe(V), and Fe(IV)], ABTS, and the  $ABTS^{\bullet+}$  radical was proposed and validated. The oxidation of ABTS by Fe(VI) ( $k = (5.96 \pm 0.9\%) \times 10^5 \text{ M}^{-1} \text{ s}^{-1}$ ), Fe(V) ( $k = (2.04 \pm 0.0\%) \times 10^5 \text{ M}^{-1} \text{ s}^{-1}$ ), or Fe(IV) ( $k = (4.64 \pm 13.0\%) \times 10^5 \text{ M}^{-1} \text{ s}^{-1}$ ) proceeds via one-electron transfer to generate  $ABTS^{\bullet+}$ , which is subsequently oxidized by Fe(VI) ( $k = (8.5 \pm 0.0\%) \times 10^2 \text{ M}^{-1} \text{ s}^{-1}$ ), Fe(V) ( $k = (1.0 \pm 40.0\%) \times 10^5 \text{ M}^{-1} \text{ s}^{-1}$ ), or Fe(IV) ( $k = (1.9 \pm 17.0\%) \times 10^3 \text{ M}^{-1} \text{ s}^{-1}$ ), respectively, via two-electron (oxygen atom) transfer to generate colorless  $ABTS_{ox}$ . At  $[ABTS]_0/[Fe(VI)]_0 > 1.0$ , experimental data and model simulation both indicated that the reaction stoichiometric ratio of Fe(VI)/ $ABTS^{\bullet+}$  increased from 1.0:1.0 to 1.0:1.2 as  $[ABTS]_0$  was increased. Furthermore, the Fe(VI)–ABTS–substrate model was developed to successfully determine reactivity of Fe(V) to different substrates ( $k = (0.7–1.42) \times 10^6 \text{ M}^{-1} \text{ s}^{-1}$ ). Overall, the improved Fe(VI)–ABTS kinetic model provides a useful tool to quantitatively probe Fe(V)/Fe(IV) behaviors in Fe(VI) oxidation and gains new fundamental insights.

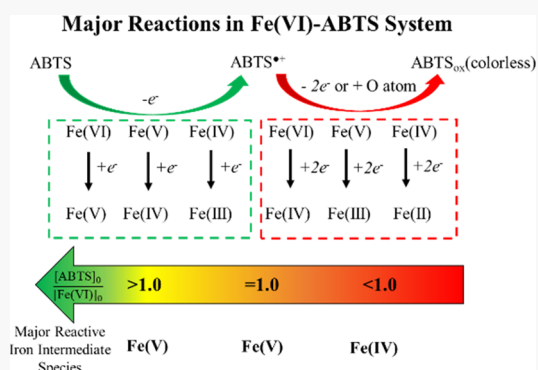
## INTRODUCTION

Over the past decade, Fe(VI) has emerged as a novel oxidant to remove contaminants from water.<sup>1,2</sup> While numerous studies have been conducted to evaluate the performance of Fe(VI) in removing different contaminants, relatively limited efforts have been devoted to understanding the mechanisms of Fe(VI) oxidation reactions that involved iron intermediate species [i.e., Fe(V) and Fe(IV)] generated via one- or two-electron transfer pathways.<sup>3,4</sup> Recently, researchers have focused on the discovery of activated-Fe(VI) systems in which activators (e.g., ammonia,<sup>5</sup> acid,<sup>6,7</sup> sulfite/thiosulfate,<sup>8–10</sup> bicarbonate,<sup>11</sup> Fe(II)/Fe(III),<sup>12</sup> Mn(II),<sup>13</sup> and carbon nanotube<sup>14</sup>) can enhance the degradation of substrates or even facilitate the removal of substrates resistant to Fe(VI) oxidation. However, the previous work heavily relied on qualitative analysis of possible reactive species formed *in situ* [radical vs Fe(V)/Fe(IV)] via quencher experiments and/or electron paramagnetic resonance spectroscopic techniques, and only limited studies<sup>15,16</sup> have attempted to quantitatively investigate the kinetic behaviors of Fe(V)/Fe(IV) for their self-decays versus oxidation of substrates.

The previous studies, even though having managed to predict the Fe(V)/Fe(IV) reactivity to the substrates based on a simplified Fe(VI)-activator system, were unable to further precisely describe the Fe(V)/Fe(IV) behaviors. The limitation

was mainly due to the difficulty in quantifying the possible chain reactions between iron species and activators, which required the accurate measurement of activator-based radicals (e.g.,  $S_2O_3^{\bullet-}$ ,  $SO_3^{\bullet-}$ , and  $SO_4^{\bullet-}$ )<sup>17</sup> formed by one-electron transfer from Fe(VI). Comparatively, 2,2'-azino-bis(3-ethylbenzothiazoline-6-sulfonic) acid (ABTS) can be oxidized by Fe(VI) to generate a persistent green-colored radical,  $ABTS^{\bullet+}$ , that can be easily measured by spectrophotometric measurements with high sensitivity.<sup>18</sup> This Fe(VI)–ABTS system could provide a tool to delineate the generation and fate of iron intermediate species Fe(V)/Fe(IV) in aqueous solution as it has been successfully utilized to explore Fe(V) reactivity under different buffer solutions (borate, phosphate,<sup>15</sup> and bicarbonate<sup>11</sup>).

ABTS has been used in quantitative determination of several oxidants (e.g., percarboxylic acid,<sup>19</sup> bromine, chlorine,<sup>20</sup> Cr(VI),<sup>21</sup> and Mn(VII)<sup>22,23</sup>) because the colorless ABTS can



Received: November 17, 2020

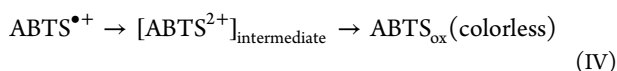
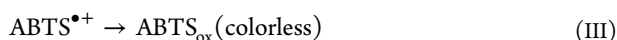
Revised: January 9, 2021

Accepted: February 10, 2021

Published: February 26, 2021



quickly react with these oxidants via one-electron transfer to yield green-colored  $\text{ABTS}^{\bullet+}$  (I). The generated  $\text{ABTS}^{\bullet+}$  can be further oxidized to  $\text{ABTS}^{2+}$  (Table S1) (II) via one-electron transfer by excess oxidants [e.g., Ce(IV), Cr(VII), and Mn(VII)] in the presence of acid.<sup>24</sup> It is also possible that  $\text{ABTS}^{\bullet+}$  can be further oxidized to colorless products (III) by certain oxidants (e.g.,  $\text{H}_2\text{O}_2$ , peroxomonosulfate, and peroxodiphosphate), and oxidation of the sulfur moiety in  $\text{ABTS}^{\bullet+}$  to form sulfoxide/sulfone-containing products was proposed but without structural identification evidence.<sup>25</sup> Meanwhile, it was reported that chlorine<sup>26</sup> could oxidize  $\text{ABTS}^{\bullet+}$  via consecutive electron transfers to form transient  $\text{ABTS}^{2+}$  intermediates via one-electron transfer, which can be further rapidly oxidized to colorless products (IV).



The Fe(VI)–ABTS system was initially proposed as a new method to determine the low concentration of Fe(VI) using excess ABTS under a reaction stoichiometric ratio of 1.0:1.0 between Fe(VI) and  $\text{ABTS}^{\bullet+}$ .<sup>18</sup> The reaction kinetics between Fe(VI) and ABTS, generating Fe(V) and  $\text{ABTS}^{\bullet+}$  ( $[\text{ABTS}]_0/[\text{Fe(VI)}]_0 > 10$ ), was then explored by the stopped-flow spectroscopy,<sup>27</sup> which could capture the rapid formation of colored  $\text{ABTS}^{\bullet+}$  and determine the reaction rate constant via pseudo-first-order fitting. The stoichiometric ratio of 1.0:1.0:1.0 among Fe(VI), ABTS, and  $\text{ABTS}^{\bullet+}$  was also confirmed.<sup>27</sup> Later, ABTS was used as an activator to enhance the degradation of diclofenac by Fe(VI) ( $[\text{ABTS}]_0/[\text{Fe(VI)}]_0 < 0.2$ ), and the enhancement was attributed to the faster oxidation by  $\text{ABTS}^{\bullet+}$  formed *in situ*.<sup>28</sup> Recently, the Fe(VI)–ABTS system at  $[\text{ABTS}]_0/[\text{Fe(VI)}]_0 = 1.0$  was proposed to be an “Fe(V)-only” system based on the assumption that there were negligible reactions between Fe(V)/Fe(IV) and  $\text{ABTS}^{\bullet+}$ .<sup>29</sup> However, the kinetic information of reactive intermediate species (i.e., Fe(V), Fe(IV),  $\text{ABTS}^{\bullet+}$ , and  $\text{ABTS}^{2+}$ ) in the Fe(VI)–ABTS system was still missing.

Therefore, on the basis that Fe(VI)–ABTS can be a useful system to evaluate Fe(V)/Fe(IV), the objective of this study was to formulate and validate an improved comprehensive model for the Fe(VI)–ABTS system that can quantitatively describe the kinetic behaviors of Fe(V)/Fe(IV) in a broad range of  $[\text{ABTS}]_0/[\text{Fe(VI)}]_0$  ratios. New experimental data were obtained by monitoring ABTS/ $\text{ABTS}^{\bullet+}$  evolution profiles using stopped-flow spectroscopy. For the first time, the oxidized ABTS product ( $\text{ABTS}_{\text{ox}}$ ) was identified using high-resolution mass spectrometry. Simulations from the kinetic model were also compared with results from previous literature studies<sup>15,27,29</sup> under different reaction conditions. Finally, the Fe(VI)–ABTS–substrate system was proposed to probe the reactivity of Fe(V) to three substrates [carbamazepine (CBZ), propranolol (PPL), and methyl phenyl sulfoxide (PMSO)] based on experimental data from a previous study.<sup>29</sup> From this work, new insights were gained by the improved kinetic simulation of Fe(V)/Fe(IV) in the Fe(VI)–ABTS system, which helped clarify some inconsistencies in previous studies.

## MATERIALS AND METHODS

**Chemicals.** Sources of chemicals and reagents are provided in the Supporting Information, Text S1. Structures and chemical properties of the target compounds are given in Table S1.

**Oxidation of ABTS by Fe(VI).** Reaction kinetics between Fe(VI) and ABTS at varied  $[\text{Fe(VI)}]_0/[\text{ABTS}]_0$  molar ratios at pH 7.0 were studied using a stopped-flow spectrophotometer that supported millisecond acquisition rates and was equipped with a UV–vis detector (Olis RSM 1000). Fe(VI) solutions were freshly prepared in 0.2 mM borate buffer (pH > 9.2) at varied concentrations of 11–100  $\mu\text{M}$ , while ABTS solutions were freshly prepared in 20 mM phosphate (pH = 6.95) at varied concentrations of 11–400  $\mu\text{M}$ . To achieve a desired  $[\text{Fe(VI)}]_0/[\text{ABTS}]_0$  ratio, different concentrations of Fe(VI) and ABTS solutions were rapidly mixed at an equal volumetric ratio to initiate the reaction and the stopped-flow spectrophotometer was operated at scan rates of 1 ms/scan (0–3.8 s), 16 ms/scan (0–5 s), or 32 ms/scan (0–50 s) for different reaction durations. Solution pH was confirmed independently by measuring it using a pH meter (Accumet Research AR 20) from mixing equal volumes of Fe(VI) (pH 9.2) and ABTS solution (pH 6.95), and the final pH was consistently at  $7.0 \pm 0.05$ .

At the lower concentrations of ABTS (<100  $\mu\text{M}$ ), the formation of  $\text{ABTS}^{\bullet+}$  and the consumption of ABTS were determined by monitoring the absorbance at 415 nm ( $\epsilon_{\text{ABTS}^{\bullet+},415\text{nm}} = 3.4 \times 10^4 \text{ cm}^{-1} \text{ M}^{-1}$ ) and 340 nm ( $\epsilon_{\text{ABTS},340\text{nm}} = 3.66 \times 10^4 \text{ cm}^{-1} \text{ M}^{-1}$ ;  $\epsilon_{\text{ABTS}^{\bullet+},340\text{nm}} = 5.9 \times 10^3 \text{ cm}^{-1} \text{ M}^{-1}$ ), respectively, and their concentrations were calculated based on a previous study.<sup>15</sup> At the higher concentrations of ABTS (150 and 200  $\mu\text{M}$ ), only the formation of  $\text{ABTS}^{\bullet+}$  was measured due to absorbance at 340 nm being too strong. The initial concentration of Fe(VI) prior to the experiment was determined by its absorbance at 510 nm ( $\epsilon_{\text{Fe(VI)},510\text{nm}} = 1.15 \times 10^3 \text{ cm}^{-1} \text{ M}^{-1}$ ) using a UV–vis spectrophotometer.

Oxidation products of ABTS by Fe(VI) were further investigated to determine the  $\text{ABTS}_{\text{ox}}$  using a solid-phase extraction procedure, followed by HPLC–high resolution mass spectrometry (LC–HRMS) analysis. Detailed analytical methods are described in Text S2.

**Oxidation of the Mixture of ABTS and  $\text{ABTS}^{\bullet+}$  by Fe(VI).** A mixed solution of ABTS and  $\text{ABTS}^{\bullet+}$  was prepared by incomplete oxidation of ABTS by peroxydisulfate (PDS) ( $[\text{ABTS}]_0 = 2[\text{PDS}]_0 = 0.6 \text{ mM}$ , pH = 7.0, and reaction time = 12 h in the dark environment) which had ~34% yield rate of  $\text{ABTS}^{\bullet+}$  in our study, in agreement with the yield rate in a previous study.<sup>30</sup> Reaction kinetics of Fe(VI) oxidation of the mixture of ABTS and  $\text{ABTS}^{\bullet+}$  were studied following the similar procedures as described above.

**Kinetic Simulation.** The kinetic simulation was conducted using the SimBiology version 5.7 in MATLAB 2018. The goodness-of-fit between simulated and experimental values was quantified by calculating the Theil’s inequality coefficient (TIC),<sup>31</sup> the normalized root mean square error (NRMSE), and the model efficiency (ME).<sup>32</sup> The local sensitivity analysis of all  $k$  values on all the species under the different reaction conditions were also performed to evaluate if all  $k$  values are influential and which of them are the most significant under certain reaction conditions. The higher sensitivity coefficient indicates that this reaction rate constant is more dominant in the evolution of certain species or overall simulation

Table 1. Proposed Reactions in the Fe(VI)–ABTS–Substrate System (Substrate = PMSO, PPL, and CBZ)<sup>a</sup>

| Reactions   | Comments   | $k$ at pH 7.0 ( $M^{-1} s^{-1}$ ) | References |
|---|--|-----------------------------------|------------|
| [1] $2HFe^{VI}O_4^- + 4H_2O \rightarrow 2H_3Fe^{IV}O_4^- + 2H_2O_2$                               |  | 26                                | 27         |
| [2] $H_2Fe^{IV}O_4^- + H_2O_2 + H^+ \rightarrow Fe^{II}(OH)_2(aq) + O_2 + 2H_2O$                  |  | $\sim 10^4$                       | 27         |
| [3] $HFe^{VI}O_4^- + Fe^{II}(OH)_2(aq) + H_2O \rightarrow H_2Fe^{V}O_4^{2-} + Fe^{III}(OH)_3(aq)$ |  | $\sim 10^7$                       | 27         |
| [4] $H_2Fe^{V}O_4^{2-} + H^+ + H_2O \rightarrow Fe^{III}(OH)_3(aq) + H_2O_2$                      |  | $10^2 (s^{-1})$                   | 52         |
| [5] $2H_2Fe^{V}O_4^{2-} + 2H_2O + 2H^+ \rightarrow 2Fe^{III}(OH)_3(aq) + 2H_2O_2$                 |  | $5.8 \times 10^7$                 | 53         |
| [6] $H_2Fe^{V}O_4^{2-} + H_2O_2 + H^+ \rightarrow Fe^{III}(OH)_3(aq) + O_2 + H_2O$                |  | $5.6 \times 10^5$                 | 54         |
| [7] $HFe^{VI}O_4^- + H_2O_2 \rightarrow H_3Fe^{IV}O_3^- + O_2$                                    |  | 10                                | 27         |
| [8] $2H_3Fe^{IV}O_4^- + 2H^+ \rightarrow 2Fe^{III}(OH)_3(aq) + H_2O_2$                            | 0– $10^3 M^{-1} s^{-1}$ based on Figure S1   | $\sim 10^3$                       | this study |
| [9] $HFe^{VI}O_4^- + ABTS + H^+ \rightarrow H_3Fe^{V}O_4^- + ABTS^{*+}$                           | based on Figure 1  | $(5.96 \pm 0.9\%) \times 10^5$    | this study |
| [10] $H_2Fe^{V}O_4^{2-} + ABTS + H^+ \rightarrow H_3Fe^{IV}O_4^- + ABTS^{*+}$                     | based on Figure 1  | $(2.04 \pm 0.0\%) \times 10^5$    | this study |
| [11] $H_3Fe^{IV}O_4^- + ABTS + H^+ \rightarrow Fe^{III}(OH)_3(aq) + ABTS^{*+} + OH^-$             | based on Figure 1 $4.6 \times 10^6 M^{-1} s^{-1}$ (pH = 1) <sup>55</sup>                                 | $(4.64 \pm 13.0\%) \times 10^5$   | this study |
| [12] $HFe^{VI}O_4^- + ABTS^{*+} + H_2O \rightarrow H_3Fe^{IV}O_4^- + ABTS_{ox}$ (oxidized ABTS)   | based on Figure 2  | $(8.5 \pm 0.0\%) \times 10^2$     | this study |
| [13] $H_2Fe^{V}O_4^{2-} + ABTS^{*+} \rightarrow Fe^{III}(OH)_3(aq) + ABTS_{ox}$ (oxidized ABTS)   | based on Figure 2  | $(1.0 \pm 40\%) \times 10^5$      | this study |
| [14] $H_3Fe^{IV}O_4^- + ABTS^{*+} \rightarrow Fe^{II}(OH)_2(aq) + ABTS_{ox}$ (oxidized ABTS)      | based on Figure 2  | $(1.9 \pm 17\%) \times 10^3$      | this study |
| [15a] $HFe^{VI}O_4^- + PMSO \rightarrow Fe^{III}(OH)_3(aq) + PMSO_2$                              | $\sim 5\text{--}10 M^{-1} s^{-1}$ (pH 8–9)   | 5                                 | 39         |
| [15b] $HFe^{VI}O_4^- + PPL \rightarrow Fe^{III}(OH)_3(aq) + P_{15b}$                              |  | 20                                | 47         |
| [15c] $HFe^{VI}O_4^- + CBZ \rightarrow Fe^{III}(OH)_3(aq) + P_{15c}$                              |  | 70                                | 48         |
| [16a] $H_2Fe^{V}O_4^{2-} + PMSO \rightarrow Fe^{III}(OH)_3(aq) + PMSO_2$                          | based on Figure 5A   | $1.25 \times 10^6$                | this study |
| [16b] $H_2Fe^{V}O_4^{2-} + PPL \rightarrow Fe^{III}(OH)_3(aq) + P_{16b}$                          | based on Figure 5B   | $1.42 \times 10^6$                | this study |
| [16c] $H_2Fe^{V}O_4^{2-} + CBZ \rightarrow Fe^{III}(OH)_3(aq) + P_{16c}$                          | based on Figure 5C   | $0.7 \times 10^6$                 | this study |
| [17a] $H_3Fe^{IV}O_4^- + PMSO \rightarrow Fe^{III}(OH)_3(aq) + PMSO_2$                            | $1.0 \times 10^5$ (pH 1–3) <sup>36</sup> 2 orders of magnitude lower than $k_{16a}$ based on Figure S17A | $\leq 1.25 \times 10^4$           | N.A.       |
| [17b] $H_3Fe^{IV}O_4^- + PPL \rightarrow Fe^{III}(OH)_3(aq) + P_{17b}$                            | 2 orders of magnitude lower than $k_{16b}$ based on Figure S17B  | $\leq 1.42 \times 10^4$           | N.A.       |
| [17c] $H_3Fe^{IV}O_4^- + CBZ \rightarrow Fe^{III}(OH)_3(aq) + P_{17c}$                            | 2 orders of magnitude lower than $k_{16c}$ based on Figure S17C  | $\leq 0.7 \times 10^4$            | N.A.       |

<sup>a</sup>Note: 1. The high-valent iron species, ABTS, and ABTS<sup>\*+</sup> species are expressed considering the major species at pH 7.0. 2. Since there was limited information about Fe(IV)'s formula, H<sub>3</sub>Fe<sup>IV</sup>O<sub>4</sub><sup>-</sup> is the proposed chemical formula of Fe(IV). 3. Equations 1–7 were based on Lee's study.<sup>27</sup> 4. N.A. = Not available.

results.<sup>33,34</sup> Detailed kinetic simulation methods are provided in Text S3. On the basis of the fitting results, the contribution ratios of each equation proposed in Table 1 to the major species in the Fe(VI)–ABTS system (i.e., Fe(VI), Fe(V), Fe(IV), ABTS, and ABTS<sup>\*+</sup>) were calculated based on the method described in Text S4.

## RESULTS AND DISCUSSION

### Kinetic Simulation of the Fe(VI) Self-Decay System (Eqs 1–8) at pH 7.0.

Fe(VI) self-decay at pH 7.0 has been carefully examined in the study by Lee et al.,<sup>27</sup> and a kinetic model including eqs 1–7 was proposed (Table 1). This kinetic model was able to accurately predict the Fe(VI) decay and H<sub>2</sub>O<sub>2</sub> generation when the initial Fe(VI) concentration ranged from 10 to 310 μM in phosphate-buffered solution. As described previously,<sup>27</sup> eq 1 represents the initiation of Fe(VI) decay in which dimerization of two mono-Fe(VI) occurs to produce two Fe(IV) and two H<sub>2</sub>O<sub>2</sub>. The formed Fe(IV) can continue to react with H<sub>2</sub>O<sub>2</sub> to produce Fe(II) and O<sub>2</sub> (eq 2) via a concerted two-electron transfer pathway. On the other hand, Fe(VI) can also react with newly generated Fe(II) from eq 2 to yield Fe(V) and Fe(III) (eq 3). Fe(V) can undergo self-decomposition via first- (eq 4) and second- (eq 5) order decays, as well as reaction with H<sub>2</sub>O<sub>2</sub> (eq 6). Equation 7 represents Fe(VI) oxidation of H<sub>2</sub>O<sub>2</sub> via two-electron transfer to generate Fe(IV) and O<sub>2</sub>.

However, Fe(IV) decay was ignored in the previous model by Lee et al. due to very limited available kinetic information.<sup>27</sup> Other research has reported that the Fe(IV) species can

undergo dimolecular decay to generate Fe(III) and H<sub>2</sub>O<sub>2</sub> at a rate constant of around  $10^6 M^{-1} s^{-1}$  based on the kinetic study of Fe(IV)–pyrophosphate by pulse radiolysis at pH 10.0.<sup>35</sup> Therefore, we added eq 8 to represent this additional sink for Fe(IV) species (Table 1). According to the sensitivity test of  $k_8$  (Figure S1) in the Fe(VI) self-decay system (eqs 1–8), Fe(VI) decay and H<sub>2</sub>O<sub>2</sub> generation were independent of the magnitude of  $k_8$  ranging from 0 to  $10^3 M^{-1} s^{-1}$ , which indicated the range boundary of  $k_8$  at pH 7.0 and provided a more precise description of Fe(IV) behavior in the Fe(VI)–ABTS system later.

### Kinetic Formulation of the Fe(VI)–ABTS System (Eqs 1–14) at pH 7.0.

We added eqs 9–14 (Table 1) into the Fe(VI) self-decay system to represent the possible interactions between high-valent iron species [Fe(VI), Fe(V), and Fe(IV)] and ABTS species (ABTS and ABTS<sup>\*+</sup>). Equations 9–11 represent ABTS oxidation by Fe(VI), Fe(V), and Fe(IV), respectively, via the one-electron transfer pathway to generate the ABTS radical cation (ABTS<sup>\*+</sup>), which were confirmed by previous studies.<sup>15,27</sup> Lee et al.<sup>27</sup> confirmed the 1.0:1.0:1.0 stoichiometric ratio for Fe(VI)/ABTS/ABTS<sup>\*+</sup> in eq 9, and Huang et al.<sup>15</sup> confirmed the contribution of Fe(V) and Fe(IV) in the Fe(VI)–ABTS system via kinetic modeling.

Equations 12–14 represent further oxidation of ABTS<sup>\*+</sup> by Fe(VI), Fe(V), and Fe(IV), respectively, likely via the oxygen transfer pathway to generate colorless products (ABTS<sub>ox</sub>) by attacking ABTS<sup>\*+</sup>. The suitability of eqs 12–14 is supported by the literature and new experimental results of this study, as discussed below. The possibility of two-electron transfer (rather than one-electron transfer) was supported by the

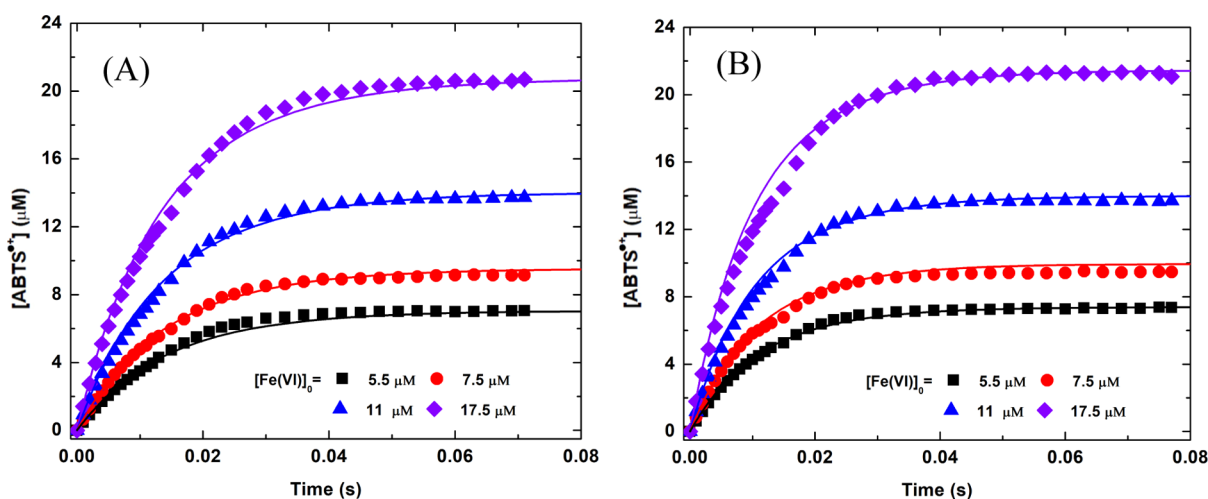


**Figure 1.** Kinetics of Fe(VI) oxidation of excess ABTS:  $[ABTS]_0 =$  (A) 150.0  $\mu\text{M}$  and (B) 200.0  $\mu\text{M}$ . Symbols: average value of parallel measurements with error bars representing one standard deviation (too small) and only selected data points shown to improve visibility; Line: model simulation. Experiments:  $n = 3$ ,  $\text{pH} = 7.0$ , 10.0 mM phosphate buffer, and 25.0  $^\circ\text{C}$ .

study by Xue et al.<sup>29</sup> in which the colored product  $ABTS^{2+}$ , which could be generated from  $ABTS^{*+}$  via one-electron transfer, could not be found in the reaction between Fe(VI) and  $ABTS^{*+}$  at neutral pH based on spectrophotometric measurements. More specifically, the experiments in our study confirmed that  $ABTS^{2+}$  ( $m/z = 257.0049$  in the electrospray ionization positive mode) was not generated in the final products of the Fe(VI)–ABTS system with the  $[ABTS]_0/[Fe(VI)]_0$  ratio ranging from 0.3 to 10 using LC-HRMS analysis (Text S2 and Figures S2 and S3). Moreover, the observed exponential decay of  $ABTS^{*+}$  and linear relationship between the calculated  $k_{\text{obs}}$  versus  $[Fe(VI)]_0$  confirmed the first-order dependence on  $[ABTS^{*+}]$  and  $[Fe(VI)]$  in Xue's study,<sup>29</sup> which validated the proposed eq 12 in the Fe(VI)–ABTS system. It is reasonable to assume that Fe(V) and Fe(IV) can display a similar oxidation mechanism (eqs 13 and 14) to Fe(VI) since high-valent iron species (e.g., Fe(IV),<sup>36–39</sup> Fe(V),<sup>40</sup> and Fe(VI)<sup>39</sup>) are known to oxidize via oxygen-atom transfer or two-electron transfer (e.g., converting sulfides/sulfoxides to the corresponding sulfoxides/sulfones).

Even more significantly, our study conducted analysis to identify the structure of oxygenated ABTS products (i.e.,  $ABTS_{\text{ox}}$ ) formed from further oxidation of  $ABTS^{*+}$ . The LC-HRMS analysis revealed that 3-ethyl-2-oxo-2,3-dihydro-1,3-benzothiazole-6-sulfonate ( $\text{C}_9\text{H}_8\text{O}_4\text{NS}_2$ ) ( $m/z = 257.9916$  in the electrospray ionization negative mode) (Figures S4 and S5) was the major oxidized product and its peak area increased dramatically from  $5.5 \times 10^5$  to  $1.2 \times 10^7$  when the  $[ABTS]_0/[Fe(VI)]_0$  ratio was decreased from 10 to 0.3. This result strongly indicates that the further oxidation of  $ABTS^{*+}$  is driven by Fe(VI) attack on the central  $\text{C}=\text{N}$  bond which leads to breakage of this bond and transfer of the O atom to the resulted electron-deficient C on the heterocyclic ring, confirming the two-electron transfer oxidation. Comparatively, the same type of product 3-methyl-2-benzothiazolinone ( $\text{C}_8\text{H}_7\text{NOS}$ ) (Table S1) was detected in the electrochemical oxidation of 2,2'-(3-methylbenzothiazolinone) azine ( $\text{C}_{16}\text{H}_{14}\text{N}_4\text{S}_2$ ) (Table S1),<sup>41</sup> which shares a very similar structure to ABTS ( $\text{C}_{18}\text{H}_{18}\text{N}_4\text{O}_6\text{S}_4$ ). The analysis of  $ABTS_{\text{ox}}$  in our work also indicates that the earlier presumption<sup>25</sup> of two-electron oxidation of  $ABTS^{*+}$  to form sulfoxide/sulfone-containing products was not correct in the ferrate system.

$\text{H}_2\text{O}_2$  generated from Fe(VI) self-decay could possibly react with ABTS/ $ABTS^{*+}$  species. However, ABTS oxidation by  $\text{H}_2\text{O}_2$  was usually catalyzed in the presence of peroxidase (e.g., lactoperoxidase<sup>42</sup> and horseradish peroxidase<sup>43</sup>) or acid,<sup>25</sup> and oxidation of  $ABTS^{*+}$  by  $\text{H}_2\text{O}_2$  was reported to be minimal in the absence of acids.<sup>25</sup> Thus, the contributions of these reactions were not considered in the Fe(VI)–ABTS system due to the reaction condition applied in this study (i.e., pH 7.0 with no peroxidases).

In order to estimate the rate constants  $k_9$ – $k_{14}$ , two different reaction conditions ( $[ABTS]_0/[Fe(VI)]_0 > 1.0$  versus  $[ABTS]_0/[Fe(VI)]_0 < 1.0$ ) were employed to probe  $k_9$ – $k_{11}$  and  $k_{12}$ – $k_{14}$ , respectively.

$[ABTS]_0/[Fe(VI)]_0 > 1.0$  (Eqs 1–11). By creating reaction conditions where  $[ABTS]_0$  was 8.6–36 times of  $[Fe(VI)]_0$ , the contribution of eqs 12–14 in influencing the  $ABTS^{*+}$  generation profile could be negligible since Fe(VI) was expected to only react with ABTS under such conditions, which was supported by sensitivity analysis discussed later in Table S10. By deploying the least-squares nonlinear regression with the constant error model in SimBiology,  $k_9$ – $k_{11}$  were successfully derived, as shown in Table 1 and Figure 1. According to the statistical analysis (ME = 0.997 and NRMSE =  $1.41 \times 10^{-2}$ ) of the experimental and simulated  $ABTS^{*+}$  concentrations (Figure S6) and goodness-of-fit based on the TIC (0.01–0.03) (Table S2), the predicted values for  $k_9$ – $k_{11}$  could successfully capture  $ABTS^{*+}$  evolution under excess ABTS conditions within 0.8 s.

It should be noted that the experimental value of  $k_9$  between Fe(VI) and ABTS was reported to be  $1.2 \times 10^6 \text{ M}^{-1} \text{ s}^{-1}$  at pH 7.0 via pseudo-first-order kinetic fitting,<sup>27,28</sup> which was  $\sim 1.8$  times of the simulated rate constant ( $5.96 \times 10^5 \text{ M}^{-1} \text{ s}^{-1}$ ) obtained from kinetic modeling of this study. The main reason for this discrepancy could be explained by the simplified reaction (i.e., only between Fe(VI) and ABTS) considered in experiments conducted by Lee et al.<sup>27</sup> and Dong et al.<sup>28</sup> which could possibly overplay the role of eq 9 in  $ABTS^{*+}$  generation as eqs 10–11 could also contribute to  $ABTS^{*+}$  generation from the oxidation of additional ABTS by Fe(V) and Fe(IV). It is also necessary to point out that the study by Huang et al.<sup>15</sup> reported the modeled  $k$  value of  $1.1 \times 10^6 \text{ M}^{-1} \text{ s}^{-1}$  between

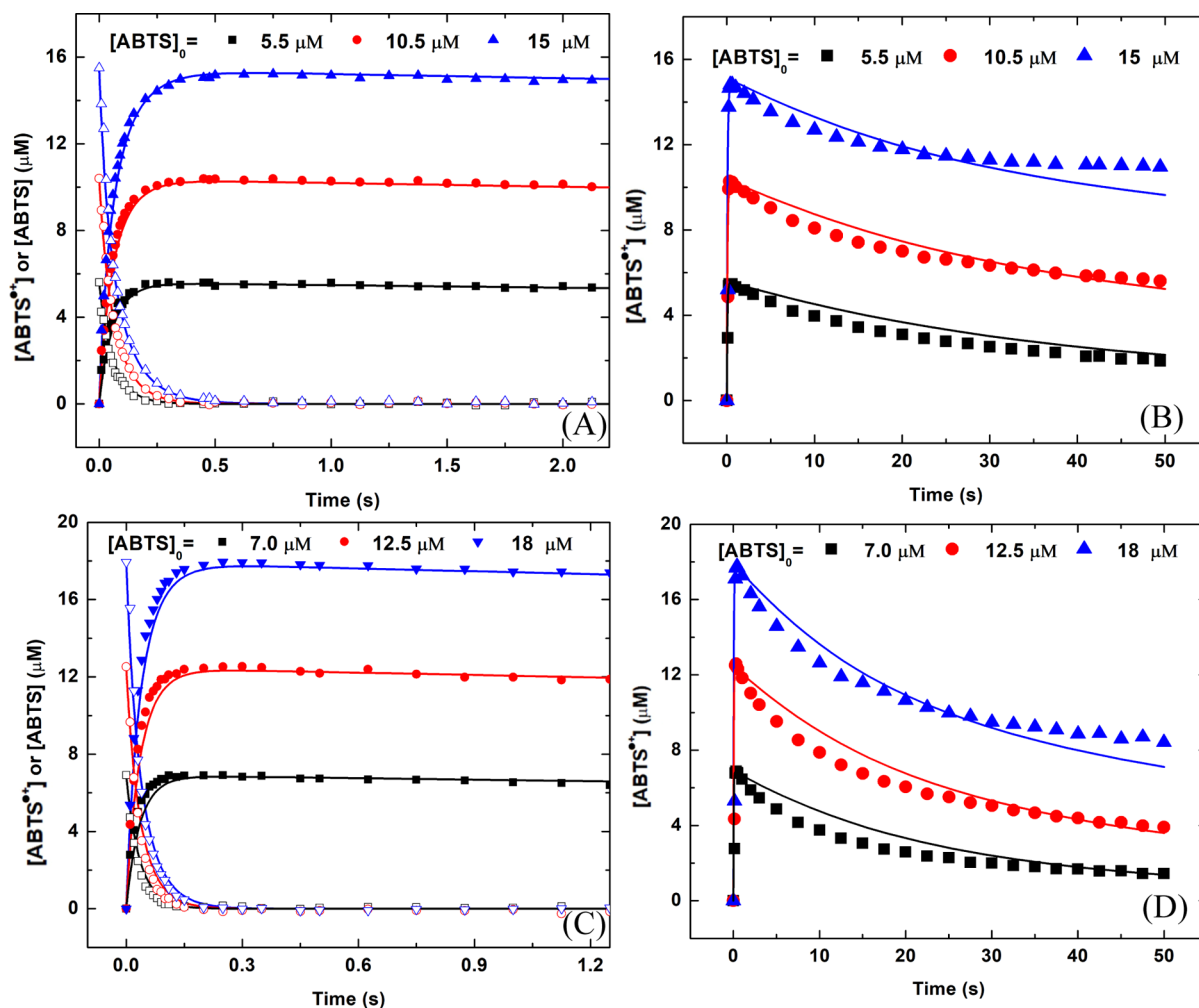


**Figure 2.** Two-stage kinetics of excess Fe(VI) oxidation of ABTS:  $[\text{Fe(VI)}]_0 = (\text{A,B}) 30.0 \mu\text{M}$  and  $(\text{C,D}) 50.0 \mu\text{M}$ . Solid (ABTS) and open (ABTS<sup>•+</sup>) symbols: average value of parallel measurements with error bars representing one standard deviation (too small) and only selected data points shown to improve visibility; Line: model simulation. Experiments:  $n = 2$ ,  $\text{pH} = 7.0$ , 10.0 mM phosphate buffer, and 25.0 °C.

Fe(VI) and ABTS in 10 mM phosphate buffer based on a kinetic model including eqs 2, 4, 5, and 9–11.

Moreover, a linear relationship between  $\log k$  (one-electron transfer) and the one-electron standard reduction potential ( $E_{(1)}^0$ ) ( $\log k(\text{one-electron}) = 6.39 (\pm 0.05) - 1.83 (\pm 0.04) \times E_{(1)}^0$ ) was initially developed based on the reactions between  $\text{HFeO}_4^-$  and six inorganic compounds<sup>3</sup> via the one-electron transfer pathway and later expanded to the  $k$  between  $\text{HFeO}_4^-$  and six organosulfur compounds<sup>44</sup> by Sharma and co-workers. By utilizing this robust equation,  $k_9$  was predicted to be  $4.7 \times 10^5 \text{ M}^{-1} \text{ s}^{-1}$  based on  $E_{(1)}^0 = 0.43 \text{ V}$  for ABTS/ABTS<sup>•+</sup>,<sup>24</sup> which was closer to the modeled value ( $5.96 \times 10^5 \text{ M}^{-1} \text{ s}^{-1}$ ) in this study. This result further suggests that  $k_9$  determined in the Fe(VI)–ABTS system by modeling in this study was likely more reasonable.

**$[\text{ABTS}]_0/[\text{Fe(VI)}]_0 < 1.0$  (Eqs 1–14).** By creating reaction conditions where  $[\text{Fe(VI)}]_0$  was two to six times of  $[\text{ABTS}]_0$ , the contribution of  $k_{12}$ – $k_{14}$  can be quantitatively evaluated by incorporating the subsequent reactions between high-valent iron species and ABTS<sup>•+</sup> (eqs 12–14). Following a similar fashion,  $k_{12}$ – $k_{14}$  were successfully derived, as shown in Table 1 and Figure 2. According to the statistical analysis (ME = 0.989–0.992 and NRMSE =  $1.53 \times 10^{-2}$  to  $3.21 \times 10^{-2}$ ) of the experimental and simulated ABTS<sup>•+</sup> concentrations

(Figure S7) and goodness-of-fit based on the TIC (0.02–0.07) (Table S3), the derived values for  $k_{12}$ – $k_{14}$  could successfully predict ABTS<sup>•+</sup> formation in the beginning (0 to 1.2 or 2.0 s) and its subsequent degradation later (0–50 s).

The reaction of ABTS with excess Fe(VI) followed two-stage oxidation with rapid generation of ABTS<sup>•+</sup> in the first stage and further slow degradation of ABTS<sup>•+</sup> in the second stage, which was also suggested by Xue's study.<sup>29</sup> The proposed Fe(VI)–ABTS model by our study further confirmed this assumption where  $k_9$  controlled the ABTS<sup>•+</sup> generation in the first 0.2 s, while  $k_{12}$  controlled the subsequent ABTS<sup>•+</sup> degradation in the following reaction time until 50 s as the sensitivity analysis shown in Table S10.

Even though the apparent rate constant between Fe(VI) and ABTS<sup>•+</sup> was reported to be  $2.33 \times 10^3 \text{ M}^{-1} \text{ s}^{-1}$ ,<sup>29</sup> which is  $\sim 2.7$  times of the simulated value ( $8.5 \times 10^2 \text{ M}^{-1} \text{ s}^{-1}$ ) in our study, it can be ascribed to the reaction solution of ABTS<sup>•+</sup> generated in Xue's study.<sup>29</sup> In Xue's study,<sup>29</sup> ABTS<sup>•+</sup> solution was prepared by dissolving 7.0 mM ABTS with 2.45 mM potassium persulfate (PDS), resulting in incomplete oxidation of ABTS since the stoichiometric ratio between PDS and ABTS is 1:2.<sup>30</sup> Thus, it is reasonable to assume that Fe(VI) was oxidizing ABTS and ABTS<sup>•+</sup> simultaneously and generated a fair amount of Fe(V)/Fe(IV) in Xue's study, where the

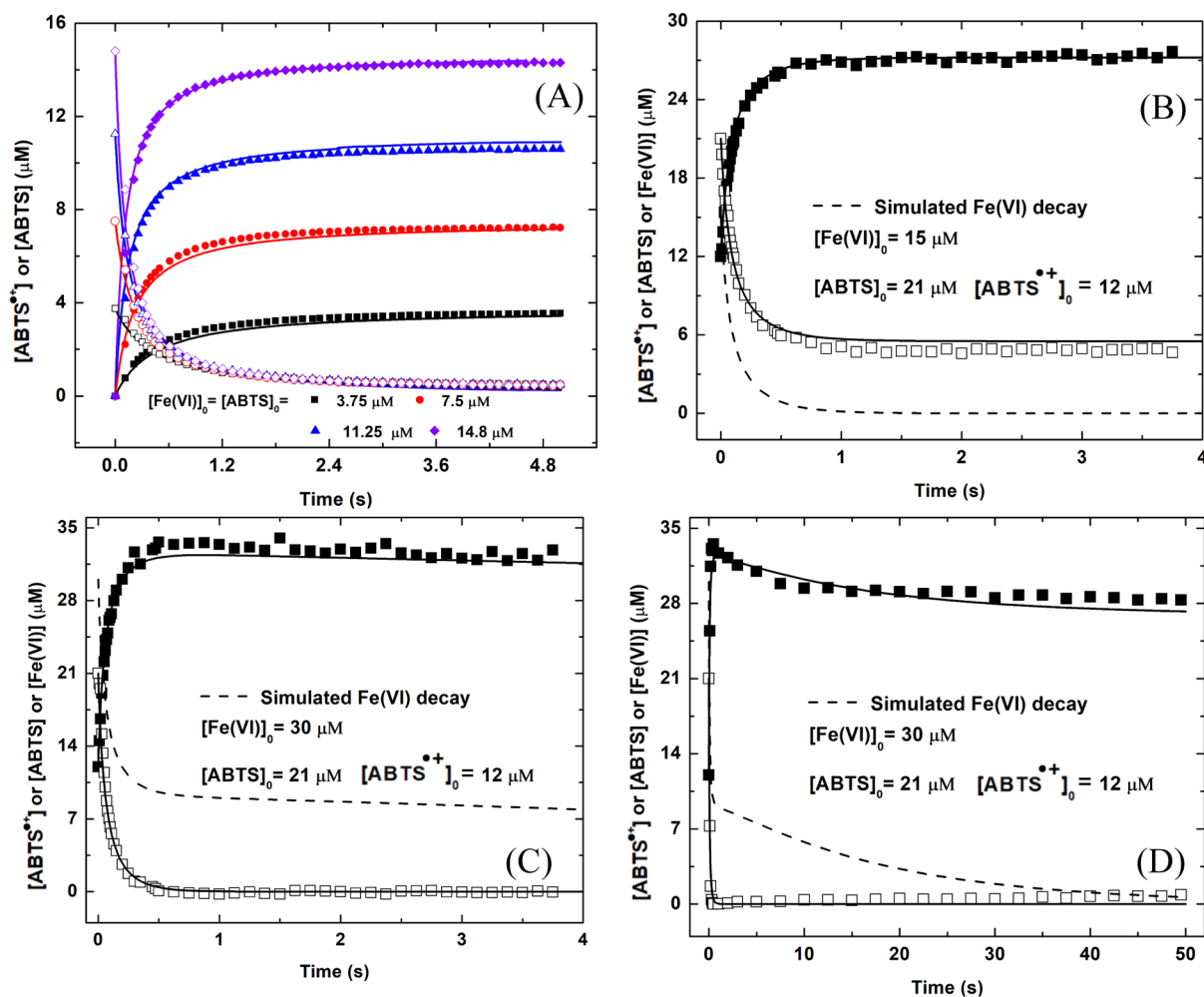


**Figure 3.** (A) Kinetics of reactions between equimolar Fe(VI) and ABTS; (B–D) kinetics of Fe(VI) oxidation of a mixture of ABTS and ABTS<sup>•+</sup>. Solid (ABTS) and open (ABTS<sup>•+</sup>) symbols: average value of parallel measurements with error bars representing one standard deviation (too small) and only selected data points shown to improve visibility; Line: model simulation. Experiments:  $n = 2$ , pH = 7.0, 10.0 mM phosphate buffer, and 25.0 °C.

apparent  $k_{2nd}$  between Fe(VI) and ABTS<sup>•+</sup> was likely overestimated owing to elevated ABTS<sup>•+</sup> concentration that existed by fast conversion of ABTS to ABTS<sup>•+</sup> in the first stage and the additional contribution by Fe(V)/Fe(IV) generated *in situ*. This can also be supported by experimental and simulated data of Fe(VI) oxidation of a mixture of ABTS and ABTS<sup>•+</sup> generated from PDS/ABTS solution in our study, as discussed in the later section (Figure 3).

**Model Validation of the Fe(VI)–ABTS System (Eqs 1–14) at pH 7.0.** As  $k_9$ – $k_{14}$  were derived from two reaction conditions ( $[ABTS]_0/[Fe(VI)]_0 > 1.0$  and  $[ABTS]_0/[Fe(VI)]_0 < 1.0$ ), additional reaction conditions were employed in experiments to generate data to further validate the robustness of these proposed rate constants.

$[ABTS]_0/[Fe(VI)]_0 = 1.0$  (Eqs 1–14). When ABTS and Fe(VI) were set to the 1.0:1.0 stoichiometric ratio at concentration ranging from 3.75 to 14.8 μM, the proposed Fe(VI)–ABTS model (eqs 1–14) could successfully simulate ABTS<sup>•+</sup> generation and ABTS degradation (Figure 3A) based on the statistical analysis (ME = 0.992–0.998 and NRMSE =  $5.27 \times 10^{-2}$  to  $5.67 \times 10^{-2}$ ) (Figure S8) and TIC (0.01–0.05) (Table S4). Moreover, the kinetic simulations by the Fe(VI)–ABTS model in this study generated very similar results compared to those in Xue’s study<sup>29</sup> ( $[ABTS]_0 = [Fe(VI)]_0 =$

20 μM and pH = 7.0) (Figure S9), which helped validate the proposed Fe(VI)–ABTS model in this study.

**Mixture of ABTS and ABTS<sup>•+</sup> (Eqs 1–14).** As shown in Figure 3B–D, the proposed Fe(VI)–ABTS model (eq 1–14) could successfully simulate ABTS<sup>•+</sup> generation and ABTS degradation in Fe(VI) oxidation of a mixture of ABTS and ABTS<sup>•+</sup> ( $[ABTS]_0 = 21 \mu\text{M}$  and  $[ABTS^{\bullet+}]_0 = 12 \mu\text{M}$ ), based on the statistical analysis (ME = 0.985–0.997 and NRMSE =  $2.93 \times 10^{-2}$  to  $3.67 \times 10^{-2}$ ) (Figures S10 and S11) and TIC (0.01–0.07) (Tables S4 and S5). In Figure 3B, the limited amount of Fe(VI) (15 μM) was expected to only oxidize ABTS in the mixture since  $k_9$  was 3 orders of magnitude higher than  $k_{12}$  and  $[ABTS]_0$  was 1.75 times of  $[ABTS^{\bullet+}]_0$ , which was confirmed by the experimental data where ABTS<sup>•+</sup> and ABTS reached their plateaus around 1 s when Fe(VI) was completely consumed ( $\Delta[ABTS] = \Delta[ABTS^{\bullet+}]$ ). Interestingly, in Figure 3C–D, ABTS<sup>•+</sup> generation and Fe(VI) (30 μM) decomposition followed two-stage kinetics. In the first stage shown in Figure 3C (0–1 s), ABTS abruptly decreased to 0, while ABTS<sup>•+</sup> increased to its maximum at 33 μM, where Fe(VI) was mainly consumed by ABTS. Subsequently, in the second stage shown in Figure 3D (1–50 s), ABTS<sup>•+</sup> was observed to decrease from 33 to 28.3 μM as modeled Fe(VI) concentration

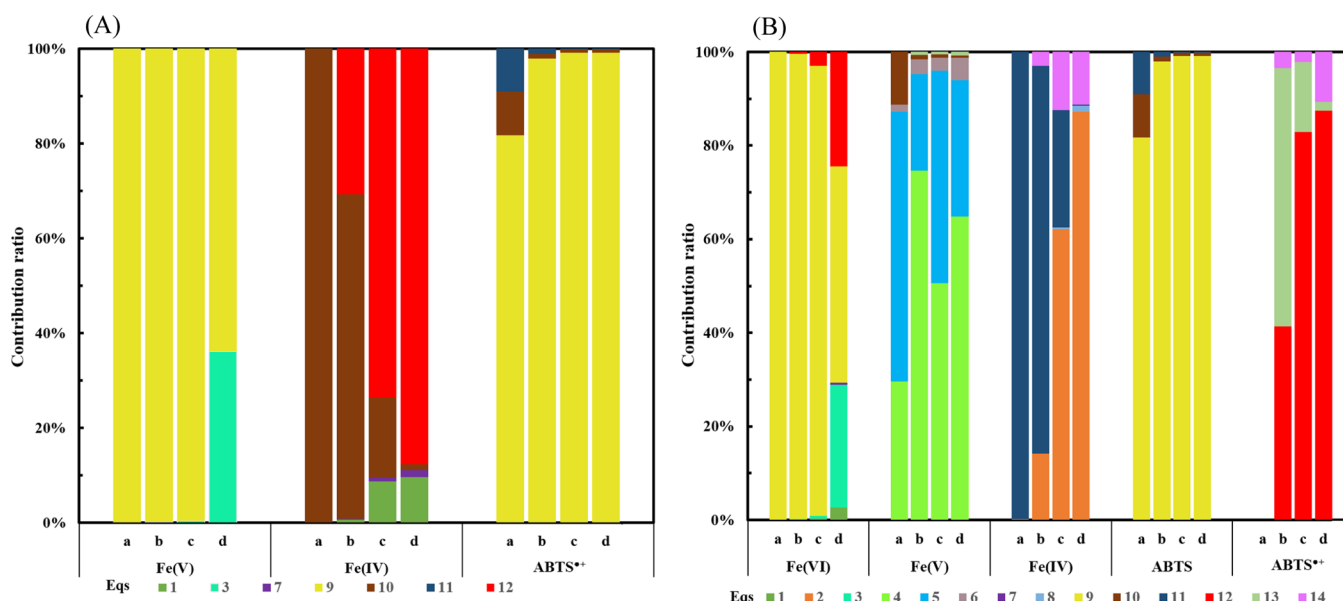


**Figure 4.** Calculated contribution ratio of eqs 1–14 to the formation (A) and degradation (B) of major species in the Fe(VI)–ABTS system under different reaction conditions a–d described in Tables S6–S10. Condition a:  $[\text{ABTS}]_0/[\text{Fe(VI)}]_0 > 1.0$ , and  $t = 0.08$  s; condition b:  $[\text{ABTS}]_0/[\text{Fe(VI)}]_0 = 1.0$ , and  $t = 5.0$  s; condition c:  $[\text{ABTS}]_0/[\text{Fe(VI)}]_0 < 1.0$ , and  $t = 1.2$  s; condition d:  $[\text{ABTS}]_0/[\text{Fe(VI)}]_0 < 1.0$ , and  $t = 50$  s. Note: the degradation percentages of  $\text{ABTS}^{\bullet+}$  generated *in situ* under conditions b, c, and d were 1.1, 3.8, and 60.1%, respectively, in Figure 4B.

decreased from 9  $\mu\text{M}$  to near zero, which indicated that the additional Fe(VI) was later consumed by  $\text{ABTS}^{\bullet+}$ .

Overall, the proposed  $k_9$ – $k_{14}$  values were first derived from model fitting to experimental data under two distinctive reaction conditions ( $[\text{Fe(VI)}]_0/[\text{ABTS}]_0 > 1.0$  and  $[\text{Fe(VI)}]_0/[\text{ABTS}]_0 < 1.0$ ) and then were further utilized to predict the evolutions of ABTS and  $\text{ABTS}^{\bullet+}$  under other reaction conditions (i.e.,  $[\text{Fe(VI)}]_0/[\text{ABTS}]_0 = 1.0$ ; mixture of ABTS and  $\text{ABTS}^{\bullet+}$ ) with excellent agreement based on TIC (0.01–0.07), ME (0.989–0.997), and NRMSE ( $1.41 \times 10^{-2}$  to  $5.67 \times 10^{-2}$ ). The robustness and accuracy of the kinetic model for the Fe(VI)–ABTS system enabled subsequent investigation of iron intermediate species [Fe(V)/Fe(IV)] under similar conditions.

**Sensitivity Analysis and Contribution Ratio of Eqs 1–14 in the Fe(VI)–ABTS System at pH 7.0.** To evaluate the importance of  $k_1$ – $k_{14}$  to the kinetic model simulation results, the local sensitivity analysis of each rate constant was performed to understand the sensitivity of the model to  $k_1$ – $k_{14}$  (especially, the newly proposed  $k_9$ – $k_{14}$ ) under the four different reaction conditions mentioned above (Tables S6–S9), and the resulted rankings are shown in Table S10. Meanwhile, the contribution of eqs 1–14 to the evolution and disappearance of Fe(VI), Fe(V), Fe(IV), ABTS, and  $\text{ABTS}^{\bullet+}$  are shown in Figure 4.

At  $[\text{ABTS}]_0/[\text{Fe(VI)}]_0 > 1.0$ , the most impactful rate constants were  $k_4$ ,  $k_5$ ,  $k_9$ ,  $k_{10}$ , and  $k_{11}$ . This confirmed the contribution of Fe(V) and Fe(IV) for  $\text{ABTS}^{\bullet+}$  evolution and the overall simulation results in Fe(VI)–ABTS, which was also supported by Huang's study.<sup>15</sup> Meanwhile, it implied that it is feasible to probe  $k_9$ – $k_{11}$  under such reaction conditions. Based on the contribution ratios of eqs 1–14 under the condition a ( $[\text{ABTS}]_0/[\text{Fe(VI)}]_0 > 1.0$ , and  $t = 0.08$  s) (Figure 4A), it indicated that eqs 9–11 all contributed to the formation of  $\text{ABTS}^{\bullet+}$  from ABTS with 81.7% from Fe(VI)-driven oxidation (eq 9), 9.2% from Fe(V)-driven oxidation (eq 10), and 9.0% from Fe(IV)-driven oxidation (eq 11). This suggested that the

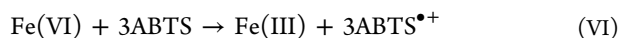
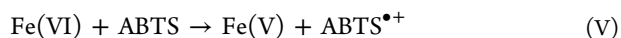
role of high-valent iron species Fe(V)/Fe(IV) in the oxidation of ABTS should not be ignored in the Fe(VI)–ABTS system.

At  $[\text{ABTS}]_0/[\text{Fe(VI)}]_0 < 1.0$ , the most important rate constants for  $\text{ABTS}^{\bullet+}$  evolution were  $k_2$ ,  $k_4$ ,  $k_9$ ,  $k_{12}$ ,  $k_{13}$ , and  $k_{14}$ , which rendered this reaction condition suitable to probe  $k_{12}$ – $k_{14}$ . Interestingly, the most influential rate constant changed from  $k_9$  to  $k_{12}$  as the reaction transitioned from the first stage ( $t = 1.2$  s) to the second stage ( $t = 50$  s), which corresponded well to  $\text{ABTS}^{\bullet+}$  formation and its decomposition shown in Figure 2. Based on the contribution ratio of eqs 1–14 under the conditions c ( $[\text{ABTS}]_0/[\text{Fe(VI)}]_0 < 1.0$ , and  $t = 1.2$  s) and d ( $[\text{ABTS}]_0/[\text{Fe(VI)}]_0 < 1.0$ , and  $t = 50$  s) (Figure 4B), the disappearance of ABTS and  $\text{ABTS}^{\bullet+}$  was mainly controlled by Fe(VI)-driven oxidation [99.1% for ABTS (eq 9) and 82.9–87.4% for  $\text{ABTS}^{\bullet+}$  (eq 12)] However, as the reaction continued from 1.2 to 50 s, Fe(IV)-driven oxidation of  $\text{ABTS}^{\bullet+}$  (eq 14) started to outcompete Fe(V)-driven oxidation of  $\text{ABTS}^{\bullet+}$  (eq 13) with contribution to the disappearance of  $\text{ABTS}^{\bullet+}$  climbing from 2.2 to 10.7%, which implied that Fe(IV) could be a critical reactive iron species to be considered at  $[\text{ABTS}]_0/[\text{Fe(VI)}]_0 < 1.0$ .

At  $[\text{ABTS}]_0/[\text{Fe(VI)}]_0 = 1.0$ ,  $k_9$ ,  $k_{10}$ , and  $k_{13}$  were the most impactful rate constants for  $\text{ABTS}^{\bullet+}$  evolution, which was expected as eqs 9, 10, and 13 were the initiation for interaction between high-valent iron species and ABTS/ $\text{ABTS}^{\bullet+}$ . Based on the contribution ratio of eqs 1–14 under the condition b ( $[\text{ABTS}]_0/[\text{Fe(VI)}]_0 = 1.0$ , and  $t = 5.0$  s) (Figure 4B), the disappearance of ABTS was still mainly controlled by Fe(VI)-driven oxidation (eq 9) with its contribution ratio at 98.0%. On the other hand, the model revealed disappearance of about 1.1%  $\text{ABTS}^{\bullet+}$  (relative to the maximum expected concentration) and the loss was controlled by both Fe(VI)-driven oxidation (eq 12) at 41.4% contribution and Fe(V)-driven oxidation (eq 13) at 55.2% contribution. This suggested that Fe(V) and Fe(VI) were both the major species responsible for the degradation of the substrates at  $[\text{ABTS}]_0/[\text{Fe(VI)}]_0 = 1.0$ .

Overall,  $k_3$ ,  $k_7$ , and  $k_8$  were considered to be the least influential rate constants in the Fe(VI)–ABTS system. The individual sensitivity test of  $k_8$  (not shown) also confirmed that simulation results were independent of  $k_8$  when ranging from 0 to  $10^3 \text{ M}^{-1} \text{ s}^{-1}$ , which agreed with the overall sensitivity analysis. Based on Figure 4B, as  $[\text{ABTS}]_0/[\text{Fe(VI)}]_0$  was increased, the major sink for Fe(IV) species would transition from its reaction with  $\text{H}_2\text{O}_2$  (eq 2) to its reaction with ABTS (eq 11). On the other hand, Fe(IV) reaction with  $\text{ABTS}^{\bullet+}$  (eq 14) only contributed to 2.9–12.4% of Fe(IV) sink, and the Fe(IV) self-decay reaction (eq 8) contributed minimally, inconsistent with the previous study<sup>29</sup> that assumed otherwise.

**Implication for the Spectrophotometric Method of Fe(VI) Detection by ABTS.** ABTS has been widely used for quantification of different types of oxidants<sup>19–23</sup> including Fe(VI), owing to its rapid reaction and simple spectrophotometric measurement with high sensitivity. However, the observed 1.0:1.0:1.0 stoichiometric ratio between Fe(VI), ABTS, and  $\text{ABTS}^{\bullet+}$  (V) ( $[\text{ABTS}]_0 = 73$  or  $80 \mu\text{M}$ ,  $[\text{Fe(VI)}]_0 < 35 \mu\text{M}$ , and 10 mM phosphate or acetate buffer) initially reported by Lee and co-workers<sup>18,27</sup> did not conform to the theoretical reaction stoichiometric ratio of 1:3 (VI) between Fe(VI) and ABTS also proposed in Lee's study.<sup>27</sup> Theoretically, the reduction of Fe(VI) to Fe(III) as the final product requires three-electron equivalents. Thus, 3 mol of ABTS is needed to generate 3 mol of  $\text{ABTS}^{\bullet+}$  in order to provide three-electron equivalents.



Lee and co-workers assumed that eqs 4–6 in Table 1, where Fe(V) can transform to Fe(III) via self-decay or reaction with  $\text{H}_2\text{O}_2$ , were the only sinks for Fe(V) formed *in situ*. However, the contribution ratio of eqs 1–14 to Fe(V) sink based on Figure 4B under condition a ( $[\text{ABTS}]_0/[\text{Fe(VI)}]_0 > 1.0$ , and  $t = 0.08 \text{ s}$ ) could not support this assumption. The contribution of Fe(V) reaction with ABTS (eq 10) to Fe(V) sink exceeded that of Fe(V) reaction with  $\text{H}_2\text{O}_2$  (eq 6) at 11.3% versus 1.5%, even though Fe(V) unimolecular and bimolecular self-decay (eqs 4 and 5) were the major Fe(V) sink pathways with their contribution ratios at 29.6 and 57.7%, respectively.

Interestingly, this observed stoichiometric ratio for Fe(VI)/ $\text{ABTS}^{\bullet+}$  started to deviate from 1.0:1.0 and increased to 1.0:1.2 as ABTS concentration was increased in this study, as shown in Figure S12A ( $[\text{ABTS}]_0 = 150$  or  $200 \mu\text{M}$ ,  $[\text{Fe(VI)}]_0 < 17.5 \mu\text{M}$ , and 10 mM phosphate buffer). A similar stoichiometric ratio of 1.0:1.18 between Fe(VI) and  $\text{ABTS}^{\bullet+}$  was also observed in Huang's study<sup>15</sup> ( $[\text{ABTS}]_0 = 100 \mu\text{M}$ ,  $[\text{Fe(VI)}]_0 < 10 \mu\text{M}$ , and 10 mM phosphate buffer). Moreover, Cyr and co-workers<sup>45</sup> observed a similar phenomenon in the Fe(VI)–ascorbic acid (AC) system, where high-valent irons [Fe(VI), Fe(V), and Fe(IV)] can transform AC to the ascorbyl radical via one-electron transfer. When the  $[\text{AC}]_0/[\text{Fe(VI)}]_0$  ratio was increased, the measured stoichiometric ratio between Fe(VI) and the ascorbyl radical was found to increase accordingly, which resembled the trend in the Fe(VI)–ABTS system. The above mentioned findings indicate that caution should be taken in the spectrophotometric method of Fe(VI) detection by ABTS, especially under low phosphate buffer concentration conditions (i.e.,  $\leq 10 \text{ mM}$ ), where  $[\text{ABTS}]_0/[\text{Fe(VI)}]_0 > 10$  may result in overestimation of Fe(VI), if assuming the 1.0:1.0 reaction stoichiometry between Fe(VI) and  $\text{ABTS}^{\bullet+}$ .

The proposed Fe(VI)–ABTS model also indicated a similar conclusion to the abovementioned findings. Based on the kinetic simulations (eqs 1–14) under Fe(VI) concentration at 2–24  $\mu\text{M}$  and ABTS concentration at 24–240  $\mu\text{M}$ , the stoichiometric ratio between simulated  $[\text{ABTS}^{\bullet+}]$  and simulated  $[\text{Fe(VI)}]$  increased from 1.0:1.0 to 1.0:1.24 when ABTS concentration was increased from 24 to 240  $\mu\text{M}$  (Figure S13). This model suggested that the optimal ratio between  $[\text{ABTS}]_0$  and maximum  $[\text{Fe(VI)}]_0$  should be lower than 2 in order to maintain the stable 1.0:1.0 stoichiometric ratio between Fe(VI) and  $\text{ABTS}^{\bullet+}$ .

Meanwhile, Dong's study<sup>28</sup> reported that  $[\text{ABTS}]_0/[\text{Fe(VI)}]_0 > 10$  was recommended for using the ABTS method for Fe(VI) determination in the presence of organic substrates (e.g., diclofenac) because an excess amount of ABTS could maintain the stability of  $\text{ABTS}^{\bullet+}$  by inhibiting it from possible reaction with the substrate. This dilemma may render difficult application of the ABTS method for determination of Fe(VI) in the presence of substrates (e.g., amino acids, phenol, and alcohol)<sup>46</sup> susceptible to  $\text{ABTS}^{\bullet+}$  oxidation, unless a new observed stoichiometry between Fe(VI) and  $\text{ABTS}^{\bullet+}$  (i.e.,  $> 1$ ) was applied when  $[\text{ABTS}]_0/[\text{Fe(VI)}]_0$  was greater than 10.

**Implication for Fe(V)/Fe(IV) Behaviors in the Fe(VI)–ABTS System.** Xue and co-workers<sup>29</sup> systematically examined the possible high-valent iron species' interactions with  $\text{ABTS}/\text{ABTS}^{\bullet+}$  at different ratios of  $[\text{ABTS}]_0/[\text{Fe(VI)}]_0$  (e.g.,  $> 1$ ,  $= 1$ , and  $< 1$ ) at pH 4–8. However, their study did not include the Fe(V)/Fe(IV) interactions with  $\text{ABTS}/\text{ABTS}^{\bullet+}$  based on the “possible overperformance” from competing reactions of Fe(V)/Fe(IV) including self-decay of Fe(V) (eqs 4 and 5), self-decay of Fe(IV) (eq 8), and reactions of Fe(V) (eq 6) and Fe(IV) (eq 2) with  $\text{H}_2\text{O}_2$ . Such assumptions may not be accurate because the competition among different sink pathways of Fe(V)/Fe(IV) depended on both reactant concentrations and reaction rate constants involved; however, the related information was not available in their study.

By utilizing the Fe(VI)–ABTS model proposed in this study, the kinetic behaviors of Fe(V)/Fe(IV) can be probed. In the system where the  $[\text{ABTS}]_0/[\text{Fe(VI)}]_0$  ratio ranged from 0.5 to 2.0 (Figure S14), Fe(V) and Fe(IV) always coexisted in the first 0.25–1.0 s. Interestingly, as ABTS concentration was increased,  $[\text{Fe(V)}]_{\text{max}}$  increased from 1.79 to 3.89  $\mu\text{M}$  with its longest lifetime to be  $\sim 1 \text{ s}$  at  $[\text{ABTS}]_0/[\text{Fe(VI)}]_0 = 1.0$ . On the other hand,  $[\text{Fe(IV)}]_{\text{max}}$  increased from 0.41 to 0.72  $\mu\text{M}$  and its lifetime decreased at  $[\text{ABTS}]_0/[\text{Fe(VI)}]_0 \geq 1.0$ , while  $[\text{Fe(IV)}]$  increased dramatically to 1.26  $\mu\text{M}$  within 3.8 s at  $[\text{ABTS}]_0/[\text{Fe(VI)}]_0 = 0.5$ .

The observations in Fe(V)/Fe(IV) simulations suggested that both Fe(V) and Fe(IV) could play important roles in substrate degradation depending on the ratio of  $[\text{ABTS}]_0/[\text{Fe(VI)}]_0$ . At  $[\text{ABTS}]_0/[\text{Fe(VI)}]_0 < 1.0$ , Fe(IV) is more likely to dominate the substrate degradation in the long run. In Dong's study,<sup>28</sup> the addition of a small amount of ABTS ( $[\text{ABTS}]_0/[\text{Fe(VI)}]_0 < 0.2$ ) could accelerate Fe(VI) oxidation of diclofenac in the course of 600 s at pH 8.0, which was explained by the possible involvement of more powerful oxidants, Fe(V) and  $\text{ABTS}^{\bullet+}$ , generated from the reaction of Fe(VI) and ABTS. However, the kinetic simulation by the model in this study suggested a different explanation. As shown in Figure S15, Fe(V) disappeared within 0.1 s, which would rule out its involvement in diclofenac degradation that lasted for 300 s. On the other hand, the  $\text{ABTS}^{\bullet+}$  lifetime only lasted for 60 s, while the Fe(IV) lifetime extended for 250 s, which

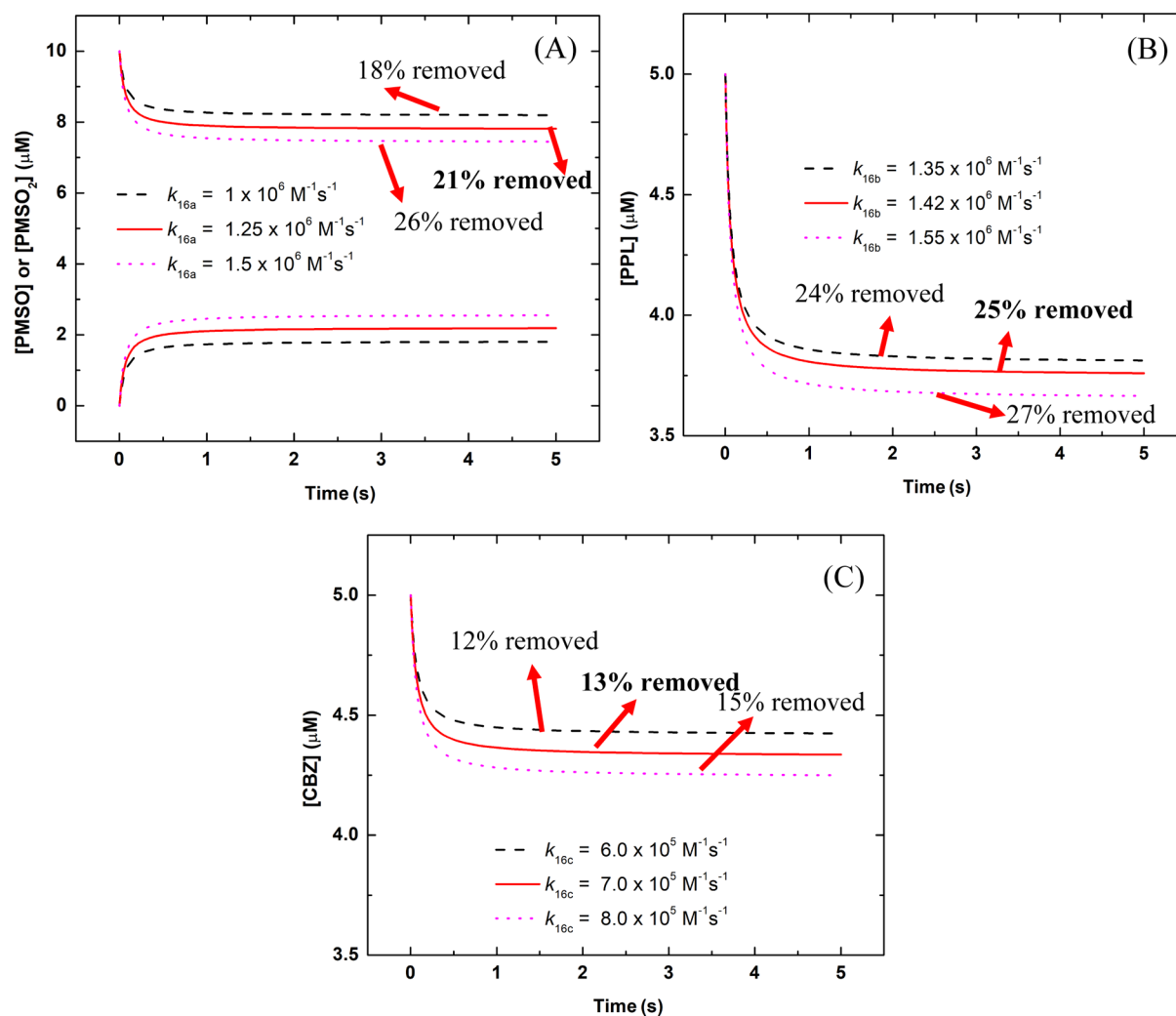


**Figure 5.** Kinetic simulation of degradation of (A) PMSO, (B) PPL, and (C) CBZ in the Fe(VI)–ABTS–substrate system based on data from a previous study.<sup>29</sup> Simulation condition:  $[\text{Fe(VI)}]_0 = [\text{ABTS}]_0 = 50 \mu\text{M}$ ,  $[\text{PMSO}]_0 = 10 \mu\text{M}$  or  $[\text{PPL}]_0$  or  $[\text{CBZ}]_0 = 5 \mu\text{M}$ , and  $t = 5.0 \text{ s}$ .

suggested that the enhanced degradation of diclofenac was more likely attributable to  $\text{ABTS}^{\bullet+}$  and Fe(IV). This could be further supported by the decreased contribution (from 14.9 to 1.9%) of Fe(V)-driven oxidation of  $\text{ABTS}^{\bullet+}$  (eq 13) and increased contribution (from 2.2 to 10.7%) of Fe(IV)-driven oxidation of  $\text{ABTS}^{\bullet+}$  (eq 14) for  $\text{ABTS}^{\bullet+}$  sink as the reaction continued under conditions c to d (Figure 4B). Future study is still needed to delineate and differentiate the roles of Fe(IV) versus  $\text{ABTS}^{\bullet+}$  in the Fe(VI)–ABTS system at  $[\text{ABTS}]_0/[\text{Fe(VI)}]_0 < 0.5$ .

At  $[\text{ABTS}]_0/[\text{Fe(VI)}]_0 > 1.0$ , Fe(V) was most likely the reactive species responsible for substrate degradation considering its higher concentration (Figure S14C,D) and higher reactivity to substrates compared to the counterpart of Fe(IV). At  $[\text{ABTS}]_0/[\text{Fe(VI)}]_0 = 1.0$ , the simulation results (Figure S14B) did not fully support that the reaction of ABTS with an equimolar amount of Fe(VI) produces an Fe(V)-only system as proposed in Xue's study,<sup>29</sup> because a lower concentration of Fe(IV) was also formed. However, Fe(V) may still be the most important iron intermediate species that is responsible for substrate decay, which will be discussed in the next section.

**Kinetic Formulation of the Fe(VI)–ABTS–Substrate System (Eqs 1–17) at pH 7.0.** Xue and co-workers<sup>29</sup> found that the degradation of 21% of PMSO, 25% of PPL, and 13%

of CBZ finished within first 5 s (the shortest time interval monitored in their study) in the Fe(VI)–ABTS system with equimolar Fe(VI) and ABTS. The authors also observed complete transformation of oxidized PMSO to  $\text{PMSO}_2$ , further confirming the roles of high-valent iron species [Fe(VI), Fe(V), and Fe(IV)] in degradation of such substrates. Therefore, the Fe(VI)–ABTS–substrate kinetic model was formulated by incorporating the interaction of high-valent iron species with each substrate (eqs 15–17) into the Fe(VI)–ABTS system (eqs 1–14). The rate constant  $k_{15}$  between Fe(VI) and a given substrate can be found in previous literature.<sup>39,47,48</sup> Even though the rate constants of Fe(IV) with the substrates were unknown, Fe(IV) was reported to react with aromatic compounds (e.g., phenol and nitrobenzene) at a rate constant of around  $10^4 \text{ M}^{-1} \text{ s}^{-1}$ ,<sup>49</sup> which was assigned to  $k_{17}$ . The rate constants  $k_{16}$  between Fe(V) and the substrate could then be successfully derived with high sensitivity (Figures 5 and S16) based on the reported removal rates. Since it has been reported that Fe(V) has much higher reactivity (2–3 orders of magnitude difference) than Fe(IV) in degradation of sulfur-containing and nitrogen-containing compounds (e.g., cyanate,<sup>50</sup> thiocyanate,<sup>4</sup> and thiourea<sup>4</sup>), it is reasonable to assume  $k_{16} > 100 \times k_{17}$ . The sensitivity test of  $k_{17}$  in the model (Figure S17) further confirmed Fe(IV)'s

negligible role in contributing to the substrate degradation since substrates' degradation was independent of  $k_{17}$  when it was at least 2 orders of magnitude lower than its counterpart  $k_{16}$ . Moreover, Fe(IV) concentration was calculated to be much lower than Fe(V) concentration at  $[ABTS]_0/[Fe(VI)]_0 = 1.0$  based on Figure S14B, which also supported the minimal contribution of Fe(IV) to degradation of substrates compared to Fe(V). Based on Figure 4B under condition b ( $[ABTS]_0/[Fe(VI)]_0 = 1.0$ , and  $t = 5.0$  s), the Fe(IV) contribution ratio to ABTS<sup>•+</sup> degradation (eq 14, 3.4%) was far less than Fe(V)-driven oxidation (eq 13, 55.2%), which also helped explain the negligible role of Fe(IV) under such a condition. Moreover, the kinetic behavior of ABTS<sup>•+</sup> simulated by the Fe(VI)–ABTS–substrate model in this study was very similar to the ABTS<sup>•+</sup> formation experimentally captured in Xue's study<sup>29</sup> (Figure S18), which further helped validate this proposed model.

Overall, substrate degradation can be finished within 0.5 s according to the simulation in the Fe(VI)–ABTS–substrate system, which required further kinetic exploration to confirm such a rapid reaction process. However, the derived  $k_{16}$  values ( $0.71 \times 10^6$  to  $1.42 \times 10^6$  M<sup>-1</sup> s<sup>-1</sup>) between Fe(V) and aromatic substrates at pH 7.0 were in good agreement with the rate constants ( $0.22 \times 10^6$  to  $1.5 \times 10^6$  M<sup>-1</sup> s<sup>-1</sup>) between Fe(V) and phenol/enrofloxacin simulated in the Fe(VI)–sulfite–substrate system at pH 6.5 and 8.0<sup>16</sup> and the rate constant ( $3.8 \times 10^5$  M<sup>-1</sup> s<sup>-1</sup>) between Fe(V) and phenol determined experimentally at pH 9.0 using pre-mix stopped-flow pulse radiolysis.<sup>51</sup> The agreement strongly indicated that the  $k_{16}$  values determined in the Fe(VI)–ABTS–substrate model were reasonable.

**Environmental Significance.** In recent years, there has been increasing attention on the enhanced roles of Fe(V)/Fe(IV) during Fe(VI) oxidation in the presence of various activators.<sup>5–13</sup> However, the kinetic behaviors (self-decay vs oxidation of substrates) of Fe(V)/Fe(IV) in the oxidation process remained unclear mainly due to the difficulty in direct and rapid measurement of these species. This study, with careful investigation of the kinetic behaviors of activator (ABTS) under varied reaction conditions, resulted in a comprehensive and robust Fe(VI)–ABTS system kinetic model, which was able to further quantitatively probe the Fe(V)/Fe(IV) kinetic behaviors and resolved some ambiguity or inconsistency in previous literature. The findings derived from Fe(VI)–ABTS system modeling also provided new guidance for the popular spectrophotometric method used for Fe(VI) determination by ABTS. Moreover, the Fe(VI)–ABTS–substrate system was proposed to evaluate the major iron intermediate species [i.e., Fe(V)] reactivity to the contaminants, which can provide a simple tool to identify the selectivity of Fe(V) in the future. Overall, this study has systemically constructed a valid kinetic model with numerous data support to examine the complexity of evolution of Fe(V)/Fe(IV) in the ABTS-enhanced Fe(VI) system. It has the potential to inspire future studies and facilitate the understanding of Fe(V)/Fe(IV) behaviors in other enhanced Fe(VI) systems and even uncover Fe(V)/Fe(IV) reactivity and selectivity to different organic pollutants based on kinetic simulation.

## ■ ASSOCIATED CONTENT

### Supporting Information

The Supporting Information is available free of charge at <https://pubs.acs.org/doi/10.1021/acs.est.0c07792>.

Details of materials and methods; contribution analysis; chemical structures and properties; TIC; sensitivity analysis; and illustrations of experimental and kinetic modeling results and analysis (PDF)

## ■ AUTHOR INFORMATION

### Corresponding Authors

Virender K. Sharma – Department of Environment and Occupational Health, School of Public Health, Texas A&M University, College Station, Texas 77843, United States; [orcid.org/0000-0002-5980-8675](https://orcid.org/0000-0002-5980-8675); Email: [vsharma@tamu.edu](mailto:vsharma@tamu.edu)

Ching-Hua Huang – School of Civil and Environmental Engineering, Georgia Institute of Technology, Atlanta, Georgia 30332, United States; [orcid.org/0000-0002-3786-094X](https://orcid.org/0000-0002-3786-094X); Email: [ching-hua.huang@ce.gatech.edu](mailto:ching-hua.huang@ce.gatech.edu)

### Authors

Cong Luo – School of Civil and Environmental Engineering, Georgia Institute of Technology, Atlanta, Georgia 30332, United States

Manasa Sadhasivan – School of Civil and Environmental Engineering, Georgia Institute of Technology, Atlanta, Georgia 30332, United States

Juhee Kim – School of Civil and Environmental Engineering, Georgia Institute of Technology, Atlanta, Georgia 30332, United States

Complete contact information is available at: <https://pubs.acs.org/doi/10.1021/acs.est.0c07792>

### Notes

The authors declare no competing financial interest.

## ■ ACKNOWLEDGMENTS

This work was supported by the projects from the National Science Foundation (CBET 1802944 and CBET 1802800).

## ■ REFERENCES

- (1) Sharma, V. K.; Chen, L.; Zboril, R. Review on high valent Fe<sup>VI</sup> (ferrate): a sustainable green oxidant in organic chemistry and transformation of pharmaceuticals. *ACS Sustainable Chem. Eng.* **2015**, *4*, 18–34.
- (2) Sharma, V. K.; Zboril, R.; Varma, R. S. Ferrates: greener oxidants with multimodal action in water treatment technologies. *Acc. Chem. Res.* **2015**, *48*, 182–191.
- (3) Sharma, V. K. Oxidation of inorganic compounds by ferrate(VI) and ferrate(V): One-electron and two-electron transfer steps. *Environ. Sci. Technol.* **2010**, *44*, 5148–5152.
- (4) Sharma, V. K. Ferrate(VI) and ferrate(V) oxidation of organic compounds: Kinetics and mechanism. *Coord. Chem. Rev.* **2013**, *257*, 495–510.
- (5) Feng, M.; Cizmas, L.; Wang, Z.; Sharma, V. K. Activation of ferrate(VI) by ammonia in oxidation of flumequine: Kinetics, transformation products, and antibacterial activity assessment. *Chem. Eng. J.* **2017**, *323*, 584–591.
- (6) Manoli, K.; Nakhla, G.; Ray, A. K.; Sharma, V. K. Enhanced oxidative transformation of organic contaminants by activation of ferrate(VI): Possible involvement of Fe<sup>V</sup>/Fe<sup>IV</sup> species. *Chem. Eng. J.* **2017**, *307*, 513–517.

- (7) Manoli, K.; Nakhla, G.; Ray, A. K.; Sharma, V. K. Oxidation of caffeine by acid-activated Ferrate(VI): Effect of ions and natural organic matter. *AIChE J.* **2017**, *63*, 4998–5006.
- (8) Zhang, J.; Zhu, L.; Shi, Z.; Gao, Y. Rapid removal of organic pollutants by activation sulfite with ferrate. *Chemosphere* **2017**, *186*, 576–579.
- (9) Sun, S.; Pang, S.; Jiang, J.; Ma, J.; Huang, Z.; Zhang, J.; Liu, Y.; Xu, C.; Liu, Q.; Yuan, Y. The combination of ferrate(VI) and sulfite as a novel advanced oxidation process for enhanced degradation of organic contaminants. *Chem. Eng. J.* **2018**, *333*, 11–19.
- (10) Shao, B.; Dong, H.; Sun, B.; Guan, X. Role of ferrate(IV) and ferrate(V) in activating ferrate(VI) by calcium sulfite for enhanced oxidation of organic contaminants. *Environ. Sci. Technol.* **2019**, *53*, 894–902.
- (11) Luo, C.; Feng, M.; Sharma, V. K.; Huang, C.-H. Oxidation of pharmaceuticals by ferrate(VI) in hydrolyzed urine: Effects of major inorganic constituents. *Environ. Sci. Technol.* **2019**, *53*, 5272–5281.
- (12) Zhao, J.; Liu, Y.; Wang, Q.; Fu, Y.; Lu, X.; Bai, X. The self-catalysis of ferrate(VI) by its reactive byproducts or reductive substances for the degradation of diclofenac: Kinetics, mechanism and transformation products. *Sep. Purif. Technol.* **2018**, *192*, 412–418.
- (13) Zhao, J.; Wang, Q.; Fu, Y.; Peng, B.; Zhou, G. Kinetics and mechanism of diclofenac removal using ferrate(VI): Roles of  $\text{Fe}^{3+}$ ,  $\text{Fe}^{2+}$ , and  $\text{Mn}^{2+}$ . *Environ. Sci. Pollut. Res.* **2018**, *25*, 22998–23008.
- (14) Pan, B.; Feng, M.; McDonald, T. J.; Manoli, K.; Wang, C.; Huang, C.-H.; Sharma, V. K. Enhanced ferrate(VI) oxidation of micropollutants in water by carbonaceous materials: Elucidating surface functionality. *Chem. Eng. J.* **2020**, *398*, 125607.
- (15) Huang, Z.-S.; Wang, L.; Liu, Y.-L.; Jiang, J.; Xue, M.; Xu, C.-B.; Zhen, Y.-F.; Wang, Y.-C.; Ma, J. Impact of phosphate on ferrate oxidation of organic compounds: An underestimated oxidant. *Environ. Sci. Technol.* **2018**, *52*, 13897–13907.
- (16) Shao, B.; Dong, H.; Feng, L.; Qiao, J.; Guan, X. Influence of [sulfite]/[Fe(VI)] molar ratio on the active oxidants generation in Fe(VI)/sulfite process. *J. Hazard. Mater.* **2020**, *384*, 121303.
- (17) Feng, M.; Jinadatha, C.; McDonald, T. J.; Sharma, V. K. Accelerated oxidation of organic contaminants by ferrate(VI): The overlooked role of reducing additives. *Environ. Sci. Technol.* **2018**, *52*, 11319–11327.
- (18) Lee, Y.; Yoon, J.; von Gunten, U. Spectrophotometric determination of ferrate (Fe(VI)) in water by ABTS. *Water Res.* **2005**, *39*, 1946–1953.
- (19) Pinkernell, U.; Lücke, H.-J.; Karst, U. Selective photometric determination of peroxy-carboxylic acids in the presence of hydrogen peroxide. *Analyst* **1997**, *122*, 567–571.
- (20) Pinkernell, U.; Nowack, B.; Gallard, H.; Von Gunten, U. Methods for the photometric determination of reactive bromine and chlorine species with ABTS. *Water Res.* **2000**, *34*, 4343–4350.
- (21) Fan, W.; Qiao, J.; Guan, X. Multi-wavelength spectrophotometric determination of Cr(VI) in water with ABTS. *Chemosphere* **2017**, *171*, 460–467.
- (22) Jiang, J.; Pang, S.-Y.; Ma, J.; Liu, H. Oxidation of phenolic endocrine disrupting chemicals by potassium permanganate in synthetic and real waters. *Environ. Sci. Technol.* **2012**, *46*, 1774–1781.
- (23) Song, Y.; Jiang, J.; Ma, J.; Pang, S.-Y.; Liu, Y.-z.; Yang, Y.; Luo, C.-w.; Zhang, J.-q.; Gu, J.; Qin, W. ABTS as an electron shuttle to enhance the oxidation kinetics of substituted phenols by aqueous permanganate. *Environ. Sci. Technol.* **2015**, *49*, 11764–11771.
- (24) Maruthamuthu, P.; Venkatasubramanian, L.; Dharmalingam, P. A fast kinetic study of formation and decay of 2, 2'-azinobis (3-ethylbenzothiazole-6-sulfonate) radical cation in aqueous solution. *Bull. Chem. Soc. Jpn.* **1987**, *60*, 1113–1117.
- (25) Venkatasubramanian, L.; Maruthamuthu, P. Kinetics and mechanism of formation and decay of 2, 2'-azinobis-(3-ethylbenzothiazole-6-sulphonate) radical cation in aqueous solution by inorganic peroxides. *Int. J. Chem. Kinet.* **1989**, *21*, 399–421.
- (26) Maruthamuthu, P.; Venkatasubramanian, L.; Dharmalingam, P. Reactions of halogens with 2, 2'-azinobis-(3-ethylbenzothiazole-6-sulphonate): Stopped-flow kinetics of formation of radical cations and dications. *Proc. - Indian Acad. Sci., Chem. Sci.* **1986**, *97*, 213–218.
- (27) Lee, Y.; Kissner, R.; von Gunten, U. Reaction of ferrate(VI) with ABTS and self-decay of ferrate(VI): Kinetics and mechanisms. *Environ. Sci. Technol.* **2014**, *48*, 5154–5162.
- (28) Dong, H.; Qiang, Z.; Lian, J.; Qu, J. Promoted oxidation of diclofenac with ferrate (Fe(VI)): Role of ABTS as the electron shuttle. *J. Hazard. Mater.* **2017**, *336*, 65–70.
- (29) Xue, M.; Wang, Z.; Sun, S.-F.; Huang, Z.-S.; Zhang, X.-X.; Ma, J.; Dong, X.-L. Mechanism investigation on the formation of high valent iron intermediate in Fe(VI) oxidation using ABTS as a probe: Effect of excess Fe(VI). *Chem. Eng. J.* **2020**, *387*, 124123.
- (30) Henriquez, C.; Aliaga, C.; Lissi, E. Formation and decay of the ABTS derived radical cation: a comparison of different preparation procedures. *Int. J. Chem. Kinet.* **2002**, *34*, 659–665.
- (31) Theil, H. *Economic Forecasts and Policy*; North-Holland Publishing Company: Amsterdam, 1961.
- (32) Esposito, G.; Frunzo, L.; Panico, A.; Pirozzi, F. Model calibration and validation for OFMSW and sewage sludge co-digestion reactors. *Waste Manage.* **2011**, *31*, 2527–2535.
- (33) Guo, X.; Minakata, D.; Niu, J.; Crittenden, J. Computer-based first-principles kinetic modeling of degradation pathways and byproduct fates in aqueous-phase advanced oxidation processes. *Environ. Sci. Technol.* **2014**, *48*, 5718–5725.
- (34) Pandis, S. N.; Seinfeld, J. H. Sensitivity analysis of a chemical mechanism for aqueous-phase atmospheric chemistry. *J. Geophys. Res.: Atmos.* **1989**, *94*, 1105–1126.
- (35) Melton, J. D.; Bielski, B. H. J. Studies of the kinetic, spectral and chemical properties of Fe(IV) pyrophosphate by pulse radiolysis. *Int. J. Radiat. Appl. Instrum., Part C* **1990**, *36*, 725–733.
- (36) Pestovsky, O.; Bakac, A. Aqueous ferryl(IV) ion: Kinetics of oxygen atom transfer to substrates and oxo exchange with solvent water. *Inorg. Chem.* **2006**, *45*, 814–820.
- (37) Bataineh, H.; Pestovsky, O.; Bakac, A. pH-induced mechanistic changeover from hydroxyl radicals to iron (IV) in the Fenton reaction. *Chem. Sci.* **2012**, *3*, 1594–1599.
- (38) Chen, J.; Xu, X.; Zeng, X.; Feng, M.; Qu, R.; Wang, Z.; Nesnas, N.; Sharma, V. K. Ferrate(VI) oxidation of polychlorinated diphenyl sulfides: Kinetics, degradation, and oxidized products. *Water Res.* **2018**, *143*, 1–9.
- (39) Pang, S.-Y.; Jiang, J.; Ma, J. Oxidation of sulfoxides and arsenic(III) in corrosion of nanoscale zero valent iron by oxygen: Evidence against ferryl ions (Fe(IV)) as active intermediates in Fenton reaction. *Environ. Sci. Technol.* **2011**, *45*, 307–312.
- (40) Li, H.; Shan, C.; Pan, B. Fe(III)-doped  $\text{g-C}_3\text{N}_4$  mediated peroxymonosulfate activation for selective degradation of phenolic compounds via high-valent iron-oxo species. *Environ. Sci. Technol.* **2018**, *52*, 2197–2205.
- (41) Janata, J.; Williams, M. B. Oxidation pathways of 2,2'-benzothiazolinone azines. I. Electrochemistry. *J. Phys. Chem.* **1972**, *76*, 1178–1183.
- (42) Reszka, K. J.; Britigan, B. E. Doxorubicin inhibits oxidation of 2, 2'-azino-bis (3-ethylbenzothiazoline-6-sulfonate) (ABTS) by a lactoperoxidase/ $\text{H}_2\text{O}_2$  system by reacting with ABTS-derived radical. *Arch. Biochem. Biophys.* **2007**, *466*, 164–171.
- (43) Kadnikova, E. N.; Kostić, N. M. Oxidation of ABTS by hydrogen peroxide catalyzed by horseradish peroxidase encapsulated into sol-gel glass.: Effects of glass matrix on reactivity. *J. Mol. Catal. B: Enzym.* **2002**, *18*, 39–48.
- (44) Sharma, V. K.; Luther, G. W.; Millero, F. J. Mechanisms of oxidation of organosulfur compounds by ferrate(VI). *Chemosphere* **2011**, *82*, 1083–1089.
- (45) Cyr, J. E.; Bielski, B. H. J. The reduction of ferrate(VI) to ferrate(V) by ascorbate. *Free Radical Biol. Med.* **1991**, *11*, 157–160.
- (46) Walker, R. B.; Everette, J. D. Comparative reaction rates of various antioxidants with ABTS radical cation. *J. Agric. Food Chem.* **2009**, *57*, 1156–1161.

(47) Anquandah, G. A. K.; Sharma, V. K.; Panditi, V. R.; Gardinali, P. R.; Kim, H.; Oturan, M. A. Ferrate (VI) oxidation of propranolol: kinetics and products. *Chemosphere* **2013**, *91*, 105–109.

(48) Hu, L.; Martin, H. M.; Arce-Bulted, O.; Sugihara, M. N.; Keating, K. A.; Strathmann, T. J. Oxidation of carbamazepine by Mn(VII) and Fe(VI): Reaction kinetics and mechanism. *Environ. Sci. Technol.* **2009**, *43*, 509–515.

(49) Mártire, D. O.; Caregnato, P.; Furlong, J.; Allegretti, P.; Gonzalez, M. C. Kinetic study of the reactions of oxoiron(IV) with aromatic substrates in aqueous solutions. *Int. J. Chem. Kinet.* **2002**, *34*, 488–494.

(50) Sharma, V. K.; O'Connor, D. B.; Cabelli, D. E. Sequential one-electron reduction of Fe(V) to Fe(III) by cyanide in alkaline medium. *J. Phys. Chem. B* **2001**, *105*, 11529–11532.

(51) Rush, J. D.; Cyr, J. E.; Zhao, Z.; Bielski, B. H. J. The oxidation of phenol by ferrate(VI) and ferrate(V). A pulse radiolysis and stopped-flow study. *Free Radical Res.* **1995**, *22*, 349–360.

(52) Rush, J. D.; Bielski, B. H. J. Decay of ferrate(V) in neutral and acidic solutions. A premix pulse radiolysis study. *Inorg. Chem.* **1994**, *33*, 5499–5502.

(53) Rush, J. D.; Bielski, B. H. J. Kinetics of ferrate(V) decay in aqueous solution. A pulse-radiolysis study. *Inorg. Chem.* **1989**, *28*, 3947–3951.

(54) Rush, J. D.; Zhao, Z.; Bielski, B. H. J. Reaction of ferrate(VI)/ferrate(V) with hydrogen peroxide and superoxide anion - A stopped-flow and premix pulse radiolysis study. *Free Radical Res.* **1996**, *24*, 187–198.

(55) Bataineh, H.; Pestovsky, O.; Bakac, A. Electron transfer reactivity of the aqueous iron(IV)-oxo complex. Outer-sphere vs proton-coupled electron transfer. *Inorg. Chem.* **2016**, *55*, 6719–6724.